IEEE Access
Multidisciplinary ⋮ Rapid Review ⋮ Open Access Journal

Received June 22, 2020, accepted June 28, 2020, date of publication July 9, 2020, date of current version July 31, 2020.

Digital Object Identifier 10.1109/ACCESS.2020.3008192

Resonant-Type Piezoelectric Screw Motor for One Degree of Freedom Positioning Platform Application

YONG ZHANG*, TAO XU*, JINSHENG HU, ZHEN HUANG, AND QIAOSHENG PAN
School of Instrument Science and Opto-Electronics Engineering, Hefei University of Technology, Hefei 230009, China

Corresponding author: Qiaosheng Pan (panqs@hfut.edu.cn)

*Yong Zhang and Tao Xu contributed equally to this work.

This work was supported in part by the Project of National Natural Science Fund of China under Grant 51705124, in part by the Fundamental and Research Funds for Central Universities under Grant JZ2018HGTB0259, and in part by the National Major Scientific Instrument Development Project: Design and Integration of Air Flotation Carrier Unit under Grant 2013YQ22074903.

ABSTRACT A resonant-type piezoelectric screw motor for one degree of freedom (1-DOF) positioning platform is proposed, fabricated, and investigated in this article. The motor comprises a driver and a screw rod. The driver is composed of four transducers, a nut seat, and a flange nut. The flange nut is bolted connected on the nut seat, and the four piezoelectric transducers are connected with the nut seat by right-angle flexible hinges. Each piezoelectric transducer comprises two piezoelectric stacks and one displacement amplifier. Driven by the four piezoelectric transducers, elliptical vibration is generated by the driver, which is used to actuate the screw rod to realize the linear movement. The driver is analyzed using the finite element analysis software ANSYS. The proposed motor and positioning platform prototype are manufactured, assembled, and tested. The performance of the developed piezoelectric screw motor shows its applicability and effectiveness for the 1-DOF positioning platform with a large force. Experiments demonstrate that the maximum velocity of this motor is 10.53 mm/s without mechanical load and the maximum output force of the platform can reach 17.19 N when the excitation voltage is 230 at 365 Hz.

INDEX TERMS Linear motor, piezoelectric actuators, positioning platform, screw driving.

I. INTRODUCTION

High-performance positioning systems have been widely used with the rapid development of the micro–nano machining, high-precision machining, and camera focusing system [1], [3], [15]. According to the position accuracy, positioning systems can be divided into coarse and precision positioning systems. Precise positioning systems have a small-displacement resolution, while coarse positioning systems are designed for large working travel and output force. Traditional coarse positioning systems are mostly driven by electromagnetic actuators. Compared with electromagnetic actuators, piezoelectric actuators have some significant advantages, such as quick response and absence of magnetic interference. Therefore, piezoelectric actuators are widely used in coarse positioning systems.

Most of piezoelectric actuators used in positioning systems usually run in a quasi-static state [1]–[7]. Li *et al.* [1] designed a positioning platform based on the inchworm principle that can achieve linear and rotary motions. The linear motion has a resolution of 0.15 μm and a maximum velocity of 105.31 μm/s. Lee *et al.* [3] presented a piezoelectric multi-axis stage based on a new stick-and-clamping actuation technology for the positioning system of the mesoscale machine tool in 2007. In a 1-DOF linear motion test, the piezoelectric multi-axis stage can achieve a speed of 1.11 mm/s with a resolution of 0.6 μm in the x and y directions. However, several application problems of the inchworm actuator, such as low running speed, complicated structure, and various driving signals, must be addressed. In addition to the quasi-static type, another class is the ultrasonic actuator, which uses the elliptical or shaky motion produced by the piezoelectric vibration bodies [8]–[15]. S.-M. Yuan *et al.* [11] proposed a screw-driven piezoelectric motor using a ''hula-hoop motion,'' in which the motor can reach 3 mm/s when the axis output force is approximately 30–40 mN. Ho and Shin *et al.* [13] developed a low-voltage drive linear ultrasonic motor with a semi-oval shaped stator

The associate editor coordinating the review of this manuscript and approving it for publication was Yingxiang Liu.

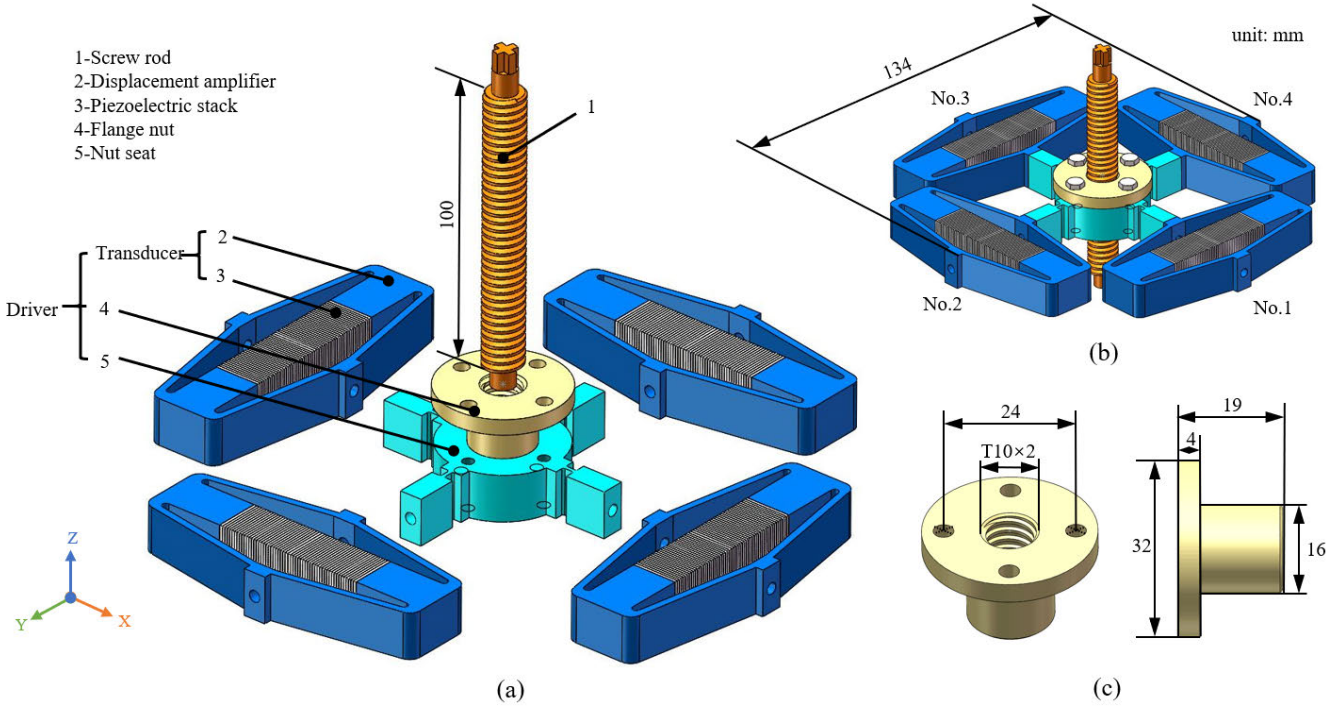

FIGURE 1. Structure of the motor. (a) Explosive view. (b) Assembly view. (c) The size of nut.

for two sine wave signal driving; the typical output of the prototype is a no-load speed of 106 mm/s and maximum thrust force of 3.33 Zhou *et al.* [14] reported a screw-driven polyhedron linear ultrasonic motor whose moving speed is 0.5–1 mm/s in the shaft direction. This motor is appropriate for the focusing system. Piezoelectric actuators driven by elliptical or shaky motion have better load performance, higher working speed, and more simple structure and signals compared with inchworm-type actuators.

A resonant piezoelectric screw motor is proposed in this article. A displacement amplifier is designed and used to amplify the small vibration to a usable degree. Right-angle flexible hinges are used to connect the piezoelectric transducers and the nut seat to ensure the transmission effectiveness of orthogonal mechanical vibration. The piezoelectric screw provides substantial axial output force at a low speed and ensures the stability and accuracy of the movement process using the crew structure. The positioning travel of the platform is related to the length of the screw rod. In this article, the positioning travel is 100 mm. The experimental results show that the piezoelectric motor can push the platform to achieve long-travel positioning of the 1-DOF platform while ensuring micron accuracy.

II. STRUCTURE AND OPERATING PRINCIPLE

A. PIEZOELECTRIC SCREW PRINCIPLE

Figure 1 shows the structure of a piezoelectric screw motor, which mainly comprises a driver as the stator and a precision screw rod as the linear mover. The driver is composed of four piezoelectric transducers, a nut seat with right-angle flexible hinges, and a flange nut. Each piezoelectric transducer comprises a displacement amplifier and two piezoelectric stacks. Each piezoelectric stack is composed of 26 layers of PZT ceramics with a dimension of 10 mm × 10 mm × 0.7 mm (produced by Hunan Jiayeda Electronics Limited Company). The PZT ceramics used in this study works under the mode. Compared with the d_{31} vibration mode, the d_{33} working mode of PZT ceramics has a large deformation under the same voltage and has high electromechanical coupling efficiency [17]. The nut seat and the four piezoelectric transducers are connected by four right-angle flexible hinges. The flange nut, the part of the driver which is in direct contact with the screw rod, is fastened to the nut seat using four fixing bolts. The thread on the screw rod is trapezoidal, with a pitch of 2 mm.

B. OPERATING PRINCIPLE

In the counterclockwise direction, the four piezoelectric transducers are labeled as No. 1, 2, 3, and 4, as shown in Figure 1(b). The four transducers are divided into two groups, namely, A and B. No. 1 and 3 are defined as group A, and No. 2 and 4 are defined as group B. The displacement amplifier is used to amplify the small displacement generated by the piezoelectric stack and fix and pre-tight the piezoelectric stacks. The displacement amplifier is transferred to the nut seat through a right-angle flexible hinge, which can reduce load structural stiffness and facilitate the displacement transmission. The vibration of the transducers is transmitted to the

linear mover through flexible hinges, and a linear movement of the screw rod is finally obtained.

The driver forms elliptical trajectories at the thread by exciting a flexural traveling wave in the flange nut. Two standing waves are essential to enable the flange nut to produce a flexural traveling wave. Figure 1(b) indicates that transducers of group A are placed on two sides of the nut seat along the x-axis direction to generate a standing wave vibration in the circumferential direction. Similarly, transducers of group B placed along the y-axis direction are used to generate vibration in the circumferential direction. The other ends of the four transducers are fixed on the base.

The driver designed in this article is a center-symmetrical structure. Thus, the resonance frequencies of the two vibration modes are easy to degenerate. Driven by the driving voltage shown in Figure 2, two standing waves will be generated on the flange nut by the two groups of transducers, then a traveling wave will be excited in the cylinder [18]. The following equation represents the traveling wave's displacement on the XY plane excited by transducers:

$$W(x,t) = \xi_0 \cos(n\theta - \omega t) \tag{1}$$

where ξ_0 is the transducer amplitude (mm), n is the number of pitch diameters on the circumference, θ is space angle, ω is the angular frequency of vibration, t is vibration time.

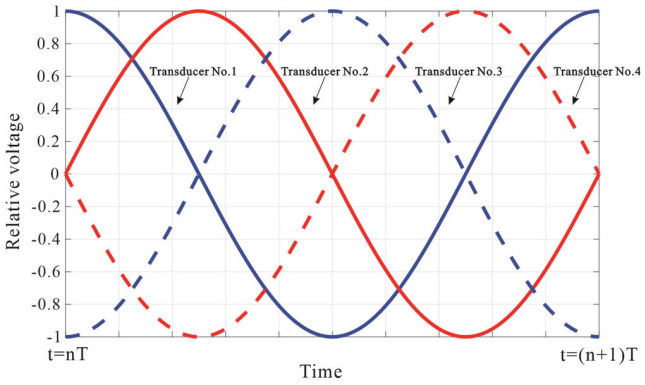

FIGURE 2. Applied voltages of the piezoelectric transducers.

The expanded view of the driver in the circumferential direction is shown in Figure 4. Figure 4 also reflects the vibration of the four piezoelectric transducers and the flange nut. h_0 represents the distance from any point P to the neutral layer of the flange nut cylinder wall.

Where R_0 refers to the radius of the cylindrical neutral layer. The relationship between the tangential vibration displacement C and the radial vibration displacement R of P satisfies the following elliptical motion equation:

$$\left(\frac{C}{n\,h_0\xi_0/R_0}\right)^2 + \left(\frac{R}{\xi_0}\right)^2 = 1 \tag{2}$$

Therefore, the trajectory of any point P on the surface of the internal thread is a standard ellipse in the XY plane, and almost no amplitude is observed in the z-axis direction [19]. Figure 3 illustrates the driving principle of the internal and external thread contact surfaces. Under a certain axial preload, the lower surface of the screw thread is in close contact with the upper surface of the flange nut thread. When the particle of the internal thread moves to the highest point of the elliptical motion, the particle will contact the thread of the rotor screw. The friction between the two contact surfaces becomes the driving force for the screw rod, which obtains a speed V_r along the circumferential tangent. The screw rotates and achieves linear movement along the z-axis as shown in Figure 5.

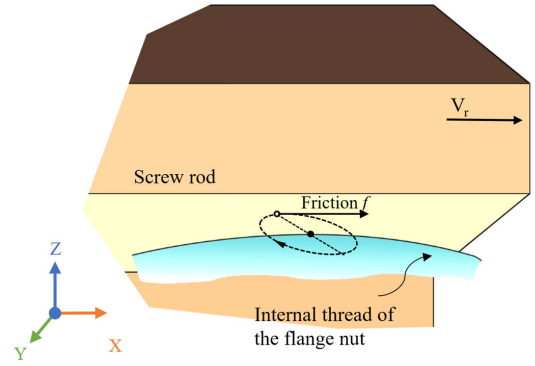

FIGURE 3. Driving principle of the contact surface.

C. 1-DOF POSITIONING PLATFORM

A 1-DOF positioning platform is designed as shown in Figure 6(a). This platform includes a piezoelectric screw motor mentioned above, four pairs of slider and guide, a lifting workbench, a base, and some auxiliary positioning parts. The workbench is in contact with the screw rod of the motor and uses rubber and a small amount of oil to reduce rotary friction damage. The sliders are fixed at the four ends of the workbench, and the guide rails are used to facilitate smooth movement. The workbench (including four sliders) is weight of 395.7g. The auxiliary positioning parts mainly include four diamond-shaped guide rail supports and rectangular bases. Two long slots are placed on both sides of each rectangular base for easy fixing to the hydraulic test bench. The travel of the workbench is related to the length of the motor screw rod and the guide rails. The manufacturing and assembly drawing of the positioning platform is shown in Figure 6(b).

III. FEM ANALYSIS AND FABRICATION

A. FEM ANALYSIS OF VIBRATION MODES

In this section, the finite element analysis software ANSYS is used to analyze the vibration modes of the driver. The vibration process of the driver in one cycle through the simulation of the driver at several time points is shown in Figure 7. Modal analysis is performed to investigate the vibration modes. The different colors represent the relative displacement of each point on the driver. During the finite element analysis, the nodes' displacement of the holes at the ends of the four piezoelectric transducers are constrained to 0 (as shown in the blue part of Figure 7) [18], [20]–[23].

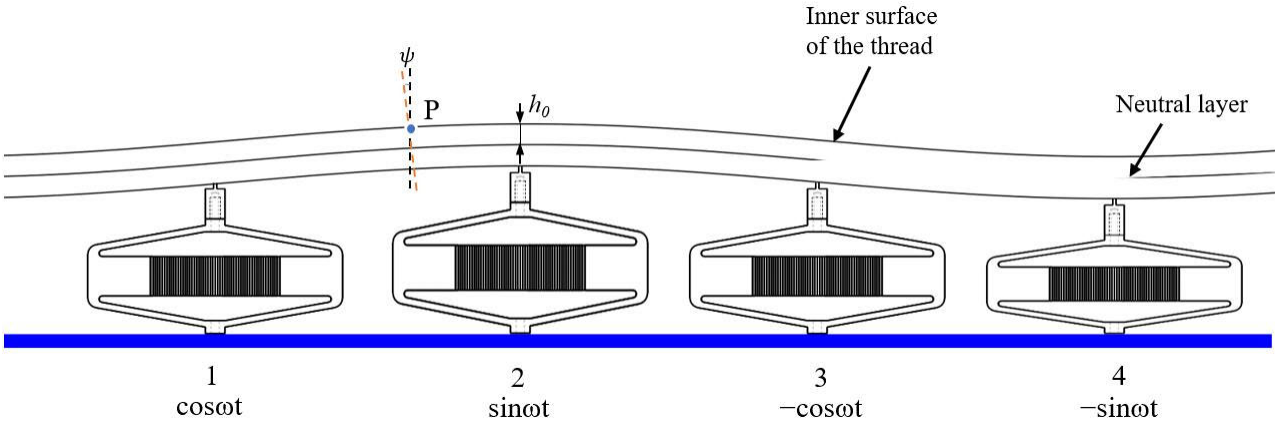

FIGURE 4. Expanded circumferential view of transducers movement.

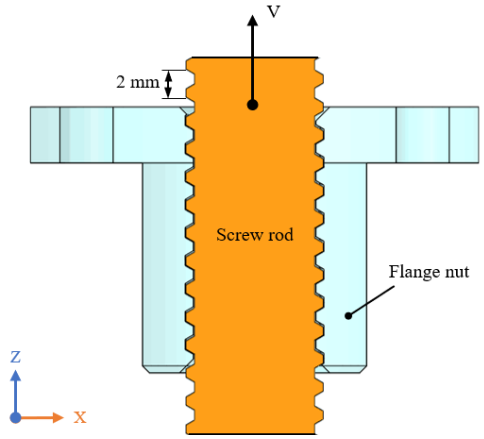

FIGURE 5. Movement of the screw rod.

The flange nut generates clockwise elliptical motion in the order of (a), (b), (c), (d). As shown in Figure 2, when the driving voltages of the four piezoelectric transducers are in the initial phase ($t = n$T), transducers No.1 and No.3 will be respectively stretched and contracted to the maximum extent. T is the period of elliptic motion of flange nut. The black point in Figure 7(a) and a small area nearby will be in close contact with the rotor screw during this time, and the friction between the two contact surfaces will drive the rotation of the screw rod and realize the upward movement of the z-axis Similarly, when $t = (n + 1/4)$ T, $(n + 1/2)$ T, $(n + 3/4)$ T, the area near the points in Figure 7(b)–(d) will contact the screw rod and drive its movement, The designed driver will vibrate as (a), (d), (c), (b) by changing the phase difference between the excitation voltages of the two sets of piezoelectric transducers. Thus, the flange nut will be prompted to implement the elliptical vibration in the counterclockwise direction, and the screw rod moves downward in the z-axis direction.

B. DESIGN OF THE DRIVER

As mentioned above, the motor consists of a driver and a screw rod. The driver is the vibration and power source of the screw rod. Therefore, its structure significantly affects the output performance of the motor. The core component of the driver is the piezoelectric transducer. The transducer consists of two piezoelectric stacks and a displacement amplifier. Lead zirconate titanate piezoelectric ceramics (PZT-4s) were used as the materials for piezoelectric stacks. The material parameters are listed in Table 1. The production process of piezoelectric stack used in this paper is mainly divided into seven steps: piezoelectric sheet polarity testing, pasting, baking, polishing, making electrical connection surfaces, polarization, and packaging [24] The displacement amplifier adopts the triangle amplification principle. This principle is designed to provide a high output displacement and a preload force to prevent the piezoelectric stacks from the tensile or shear force.

TABLE 1. The material parameters for the PZT-4s ceramics.

property	Tensor(in order of *x, y, z, xy, xz, yz*)
Piezoelectricity ($C\ m^{-2}$)	$\begin{bmatrix} 15.1 & 0 & 0 \\ -5.2 & 0 & 0 \\ -5.2 & 0 & 0 \\ 0 & 12.7 & 0 \\ 0 & 0 & 0 \\ 0 & 0 & 12.7 \end{bmatrix}$
Stiffness ($10^{10} \times m^{-2}$)	$\begin{bmatrix} 13.9 & 7.78 & 7.43 & 0 & 0 & 0 \\ 7.78 & 13.9 & 7.43 & 0 & 0 & 0 \\ 7.43 & 7.43 & 11.5 & 0 & 0 & 0 \\ 0 & 0 & 0 & 3.06 & 0 & 0 \\ 0 & 0 & 0 & 0 & 2.56 & 0 \\ 0 & 0 & 0 & 0 & 0 & 2.56 \end{bmatrix}$
Permittivity ($F\ m^{-1}$)	$\begin{bmatrix} 728.5 & 0 & 0 \\ 0 & 728.5 & 0 \\ 0 & 0 & 634.7 \end{bmatrix}$

A force of about 750 N is applied to the output end of the displacement amplifier to support its opening. Then the stack is placed inside the displacement amplifier, and the PZT stack is pre-tightened by stuffing the two ends of the stack with aluminum oxide of appropriate thickness. preloading force applied on the stack is about 3000N-4000N.

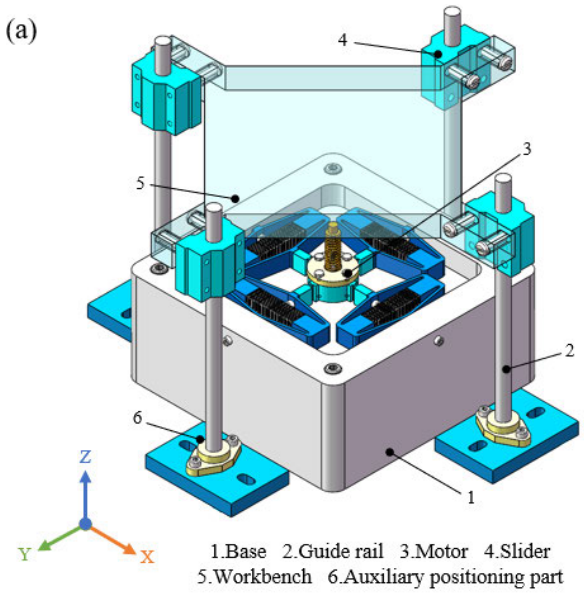

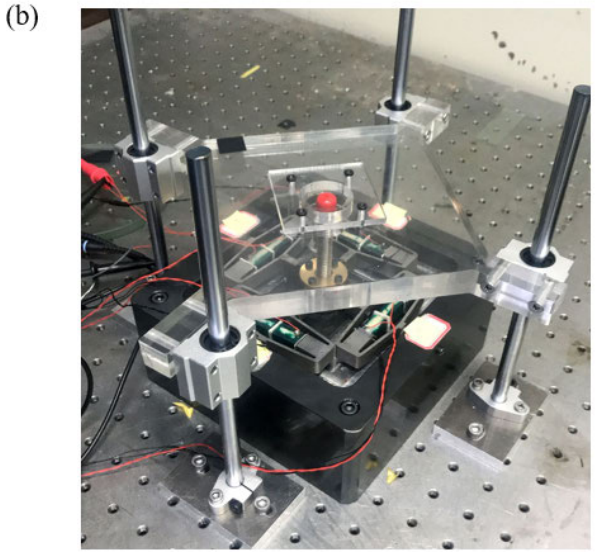

FIGURE 6. Prototype of a 1-DOF positioning platform. (a) Model diagram. (b) Assembly drawing.

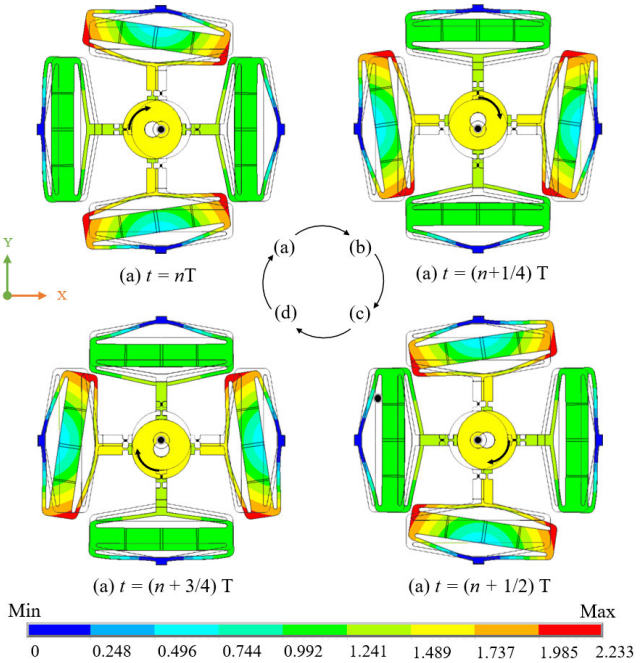

FIGURE 7. Shape change of the designed driver.

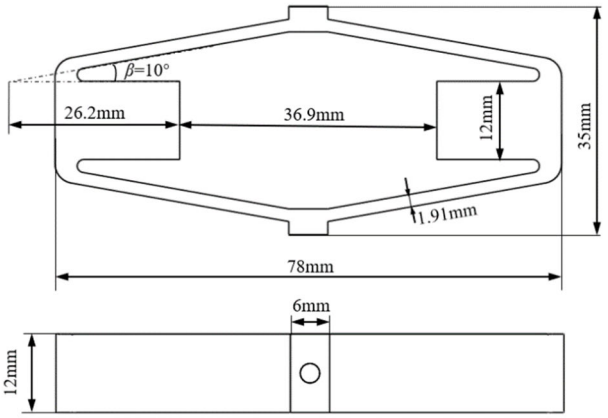

FIGURE 8. Size diagram of the transducer.

The output displacement of the displacement amplifier is determined by the amplification ratio and the actual displacement of the piezoelectric stack in the amplifier. It should be mentioned that the output displacement of the stack in the amplifier is inversely proportional to the stiffness of the amplifier and the amplification ratio is inversely proportional to β. β represents the angle between the rigid link and the horizontal line, as shown in Figure 8. Therefore, the β and stiffness are the two crucial points in the design of the displacement amplifier [25].

To increase the amplification ratio, the β needs to be reduced as much as possible. Since the dimensions of the piezoelectric stack is determined, the influence of the β on the preload force also needs to be considered. The smaller the stiffness of the displacement amplifier is, the smaller the displacement loss of the piezoelectric stack is, which means larger output displacement would be generated by the amplifier. However, if the stiffness is too small, it will cause great stress and affect the service life of the displacement amplifier.

Manganese steel is selected as the material of the displacement amplifier. The density, elastic modulus and poisson's ratio of manganese steel are 7840 kg/m^3, 200 GPa and 0.2 respectively. The specific size parameters are shown in Figure 8.

The nut seat is also made of manganese steel. The dimensions of flange nut made of brass are shown in Figure 1(c). The density, elastic modulus and poisson's ratio of brass are 8470 kg/m^3, 105 GPa and 0.343 respectively.It is custom-made with high thread accuracy, which can fully contact the screw rod and provide sufficient friction. The overall size of the driver is shown in Figure 1(b).

The thread on the screw rod is trapezoidal, and the size of the screw rod which is made of stainless steel is shown in Figure 1(a). Thus, the driver can drive the screw rod to achieve linear movement in the z-axis direction.

IV. EXPERIMENT AND RESULT

A. IMPENDANCE CHARACTERISTICS OF THE DRIVER

An impedance analyzer (LCR-8101, GW Instek, China) is used to test the two groups of piezoelectric transducers (No.1.3 and No.2.4) of the driver. The test frequency range is set to 100–1000 Hz, and the test voltage is set to be 1 $V_{p\text{-}p}$. The test results in Figure 9 show that the resonance frequencies of transducer groups A and B are 374 and 370 Hz, respectively. These frequencies are slightly different from the simulation result of 375 Hz, and the relative errors are approximately 0.3% and 1.1%. The results are caused by the parameter tolerance during production, different preloads on the ends of the piezoelectric transducers and stacks during assembly, and disparities between the simulation and fabrication in modeling. Due to the piezoelectric stacks and the displacement amplifiers are manufactured by ourselves in the laboratory, admittance of transducers 1,3 and transducers 2,4 are not strictly equal to each other.

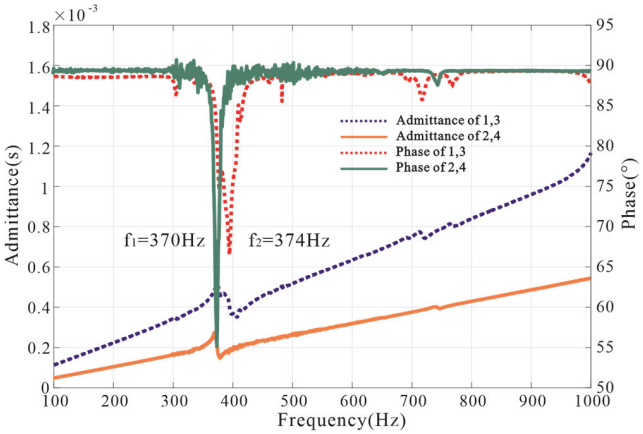

FIGURE 9. Vibration characteristics of the driver.

B. EXPERIMENTAL SETUP FOR THE MOTOR AND POSITIONING PLATFORM

A test platform of the motor and positioning platform was established as shown in Figure 10. Four alternating voltages with the same frequency and a phase difference of $\pi/2$ were supplied by the signal generator (DG 1022U, Rigol, USA) and magnified with a high-power amplifier (LYF-800AS, Nantong Long Yi Electronic Technology Co.,Ltd, China) in this article. The oscilloscope was used to monitor the driving voltage of the piezoelectric stacks, record the voltage on the cement resistor in the detection circuit, and then calculate the current in the circuit. A laser displacement sensor (ILD 2300-2, Micro-Epsilon, Germany) was fix on a magnetic gauge holder to record the linear displacement of the screw rod or the workbench in the z-axis direction and calculate

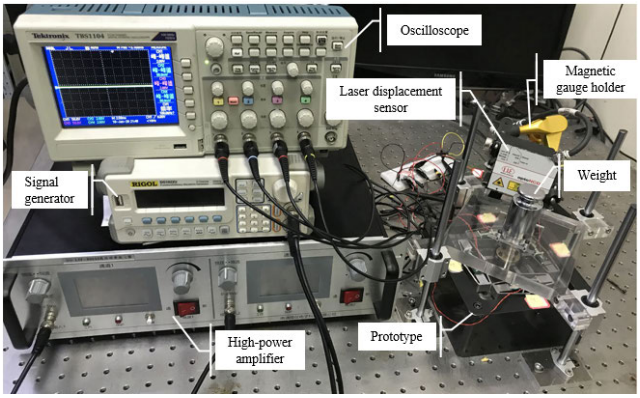

FIGURE 10. Experimental setup for the prototype.

the speed characteristics. The main function of the weight is to test the load performance of the positioning platform. Considering the actual manufacturing errors of the four transducers, the amplitude of each transducer varies despite the application of the same voltage. The excitation voltages of the transducers must be adjusted to achieve the same amplitude in the x- and y-axis directions to ensure the reliability of the experiments.

C. SPEED CHARACTERISTICS OF THE MOTOR

The linear speed of the screw rod in the z-axis direction without workbench was first measured. As previously mentioned, the laser displacement sensor was used to measure the displacement of the screw rod and calculate the speed. Figure 11 shows the relation curve of the screw rod velocity under different frequencies. The maximum moving speed was obtained when the driving frequency was 365 Hz. This frequency is slightly lower than the measured frequency with the impedance meter as shown in Figure 9 due to the slight decrease in the resonance frequency when the screw rod is loaded. At this frequency, the temperature of the PZT stacks raised from 27 °C to 31 °C after the motor operated continuously for 30 minutes. The relationship between the linear speed of the screw rod and the excitation voltage with the driving frequency of 365 Hz was also studied as shown in Figure 12. The linear movement speed is positively correlated to the excitation voltage, which can remarkably reach 10.53 mm/s at 230 $V_{p\text{-}p}$.

D. PERFORMANCE OF THE POSITIONING PLATFORM

Experiments on load performance and positioning accuracy were presented and conducted. In the case of no load, the maximum noise generated by the motor was 79 dB when the workbench moved steadily. The decibel meter was about 30mm away from the motor. The relationship between the load force and the positioning platform velocity obtained by measuring the z-axis direction movement of the workbench was studied as shown in Figure 13. The loads include the weight of the platform. During the experiment process, the excitation voltage and driving frequency were

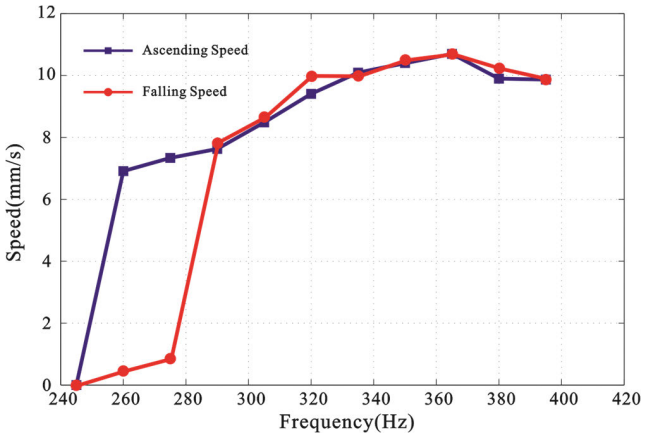

FIGURE 11. Speed of the screw rod at different frequencies.

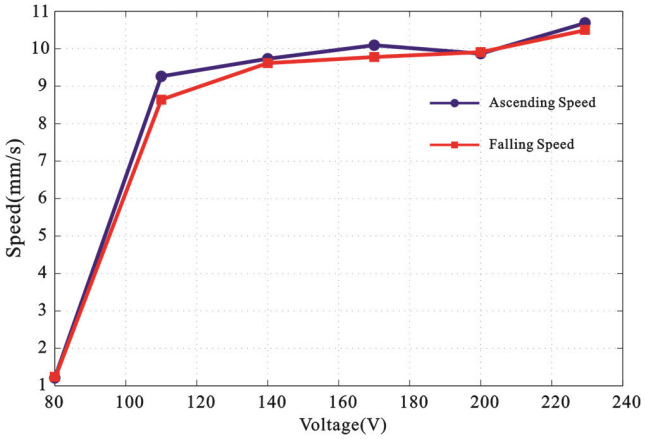

FIGURE 12. Speed of the screw rod under different excitation voltages.

respectively set to 230 $V_{p\text{-}p}$ and 365 Hz. Considering the influence of the workbench gravity, the falling speed of this workbench is larger than its ascending speed under the same load. The speed of the positioning platform increases with the load within a certain range. As the load continues to increase, the speed of the positioning platform gradually decreases until it becomes unstable. The positioning platform can remarkably maintain stable ascending and falling speeds of 2.87 and 4.82 mm/s, respectively, under the load of 17.19 N.

Figure 14 shows the characteristic of the linear motion displacement of the designed positioning platform under no-load state, with a driving voltage of 230 $V_{p\text{-}p}$ and a frequency of 365 Hz. The displacement of the positioning platform ascends or descends stepwise with the fluctuation, and the ascending or descending time of each step is approximately equal to the period of the driving signal.

In the whole ascending process, the resolution of ascending is approximately 20.22 μm. In the whole falling process, the resolution of falling is approximately 21.96 μm.

E. EFFICIENCY OF THE POSITIONING PLATFORM

The efficiency of the positioning platform was tested and studied as shown in Figure 15. In the driving circuit of the

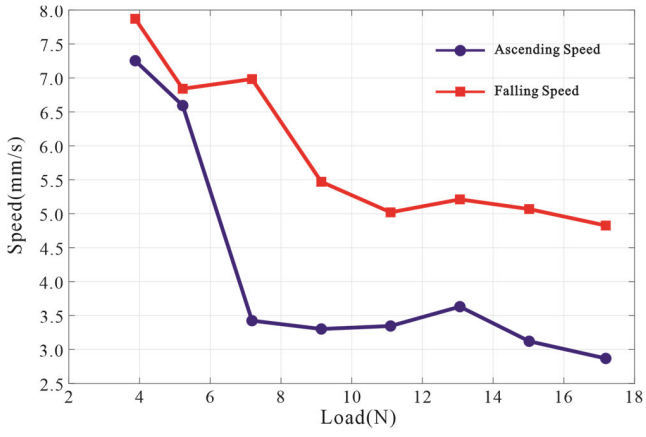

FIGURE 13. Load performance of the positioning platform.

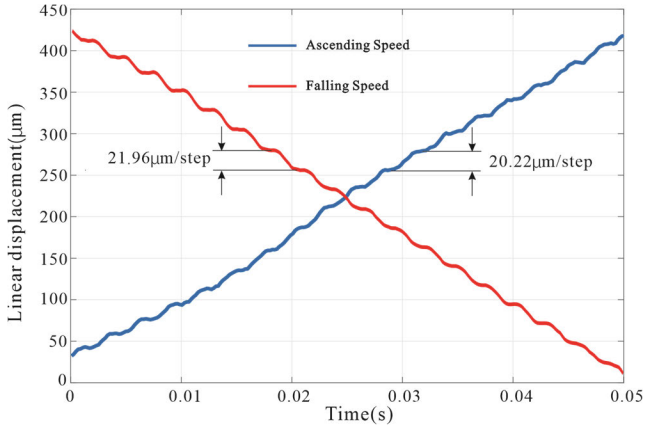

FIGURE 14. Characteristic of the linear motion displacement.

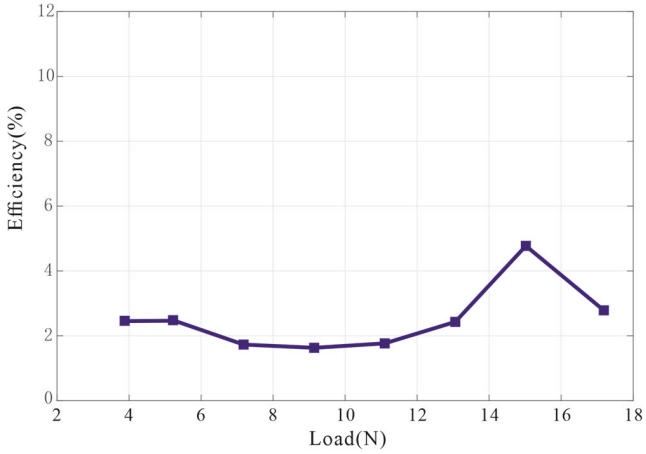

FIGURE 15. Working efficiency under different loads.

piezoelectric transducer, a cement resistance with a small resistance value is connected with piezoelectric stacks in series, and the current value of the whole circuit can be obtained by the oscilloscope. The input electric power $P_i = UI\Delta t/T$ can be calculated by the data saved by the oscilloscope. In order to facilitate the calculation, it is considered that the positioning platform moves at a uniform speed in the process of motion. Therefore, the output mechanical power

TABLE 2. Comparison between the designed motor and the previous piezoelectric motor.

Reference	Year	Maximum Velocity	Output force	Principle	Frequency	Driving Voltage
[1]	2014	105.31μm/s	4.9N	Inchworm	26Hz	100V
[12]	2016	2.137mm/s	0.16N	Elliptical motion	1.58kHz	16V
[13]	2013	106mm/s	3.33N	Elliptical motion	41.5kHz	16V
[28]	2015	32000μrad/s	11.76N	Inertial	100Hz	100V
Our motor	2020	10.53mm/s	17.19N	Elliptical motion	365Hz	230V

can be obtained by using the formula $P_o = Fv = mgv$, and the ratio of the two is the working efficiency.

The result illustrates that the working efficiency continuously changes with the turn of the movement direction and the different loads. Moreover, the efficiency of the positioning platform is positively related to the load within a certain range.

The maximum efficiency during the ascending movements is 4.8%.

V. CONCLUSIONS

A new resonant-type piezoelectric screw motor for a 1-DOF positioning platform is proposed. The designed 1-DOF positioning platform can realize a wide range of movements in the z-axis direction with a large output force. Four piezoelectric transducers are used in the designed motor. An elliptical vibration is obtained in the driver by combining the two orthogonal mechanical vibrations. The friction between the thread contact surfaces drives the rotation of the screw rod to realize linear movement. The motor and positioning platforms are manufactured to test and study the working characteristics. The experimental results show that the maximum velocity of the designed motor is 10.53 mm/s without load. The maximum output force of the positioning platform driven by the proposed motor is 17.19 N, and the minimum linear motion resolution is approximately 20.7 μm. Table 2 illustrates the performance parameters of some piezoelectric actuators mentioned in this article. The piezoelectric screw motor proposed in this article has the best load performance and can expand the application of piezoelectric actuators in coarse positioning systems.

However, tedious work must be done to improve the design practicality. Miniaturization and integrated design are also crucial in the subsequent design.

REFERENCES

[1] J. Li, H. Zhao, X. Qu, H. Qu, X. Zhou, Z. Fan, Z. Ma, and H. Fu, "Development of a compact 2-DOF precision piezoelectric positioning platform based on inchworm principle," *Sens. Actuators A, Phys.*, vol. 222, pp. 87–95, Feb. 2015.

[2] Y. Peng, H. Wang, S. Wang, J. Wang, J. Cao, and H. Yu, "Design and experimental validation of a linear piezoelectric micromotor for dual-slider positioning," *Microsyst. Technol.*, vol. 23, no. 7, pp. 2363–2370, Jul. 2017.

[3] S. W. Lee, K.-G. Ahn, and J. Ni, "Development of a piezoelectric multi-axis stage based on stick-and-clamping actuation technology," *Smart Mater. Struct.*, vol. 16, no. 6, pp. 2354–2367, Dec. 2007.

[4] P. Lambert, A. Valentini, B. Lagrange, P. De Lit, and A. Delchambre, "Design and performances of a one-degree-of-freedom guided nano-actuator," *Robot. Comput.-Integr. Manuf.*, vol. 19, nos. 1–2, pp. 89–98, Feb. 2003.

[5] J. Li, H. Zhao, H. Qu, T. Cui, L. Fu, H. Huang, L. Ren, and Z. Fan, "A piezoelectric-driven rotary actuator by means of inchworm motion," *Sens. Actuators A, Phys.*, vol. 194, pp. 269–276, May 2013.

[6] H. Lu, J. Zhu, Z. Lin, and Y. Guo, "An inchworm mobile robot using electromagnetic linear actuator," *Mechatronics*, vol. 19, no. 7, pp. 1116–1125, Oct. 2009.

[7] D. Kang, M. G. Lee, and D. Gweon, "Development of compact high precision linear piezoelectric stepping positioner with nanometer accuracy and large travel range," *Rev. Sci. Instrum.*, vol. 78, no. 7, Jul. 2007, Art. no. 075112.

[8] S.-T. Ho and S.-J. Jan, "A piezoelectric motor for precision positioning applications," *Precis. Eng.*, vol. 43, pp. 285–293, Jan. 2016.

[9] L.-K. Chang and M.-C. Tsai, "Design of single-phase driven screw-thread-type ultrasonic motor," *Rev. Sci. Instrum.*, vol. 87, no. 5, May 2016, Art. no. 055002.

[10] J. Hong, J. Long, and X. Zhike, "Design and characteristic study of large torque micro-nano platform based on piezoelectric stack," in *Proc. 17th Int. Conf. Electr. Mach. Syst. (ICEMS)*, Oct. 2014, pp. 2697–2700.

[11] S.-M. Yuan, H.-Y. Zha, and X.-C. Chu, "The principle and structure of a screw drive piezoelectric motor," in *Proc. Symp. Piezoelectr., Acoustic Waves, Device Appl. (SPAWDA)*, Dec. 2009, p. 106.

[12] S.-T. Ho and W.-H. Chiu, "A piezoelectric screw-driven motor operating in shear vibration modes," *J. Intell. Mater. Syst. Struct.*, vol. 27, no. 1, pp. 134–145, Jan. 2016.

[13] S.-T. Ho and Y.-J. Shin, "Design of a semi-oval shaped ultrasonic motor," *Int. J. Autom. Technol.*, vol. 7, no. 5, pp. 537–543, Sep. 2013.

[14] T. Zhou, Y. Zhang, Y. Chen, C. Lu, D. Fu, Y. Li, and X. Hu, "A nut-type ultrasonic motor and its application in the focus system," *Chin. Sci. Bull.*, vol. 54, no. 20, pp. 3778–3783, Oct. 2009.

[15] P. Vasiljev, D. Mazeika, and G. Kulvietis, "Modelling and analysis of omni-directional piezoelectric actuator," *J. Sound Vib.*, vol. 308, nos. 3–5, pp. 867–878, Dec. 2007.

[16] X. Hou, H. Lee, C. Ong, and S. Lim, "Development and numerical characterization of a new standing wave ultrasonic motor operating in the 30–40 kHz frequency range," *Ultrasonics*, vol. 53, no. 5, pp. 928–934, 2013.

[17] Y. Liu, W. Chen, J. Liu, and S. Shi, "Actuating mechanism and design of a cylindrical traveling wave ultrasonic motor using cantilever type composite transducer," *PLoS ONE*, vol. 5, no. 4, Apr. 2010, Art. no. e10020.

[18] Y. Liu, J. Yan, L. Wang, and W. Chen, "A two-DOF ultrasonic motor using a longitudinal–bending hybrid sandwich transducer," *IEEE Trans. Ind. Electron.*, vol. 66, no. 4, pp. 3041–3050, Apr. 2019, doi: 10.1109/tie.2018.2847655.

[19] Y. Liu, W. Chen, J. Liu, and S. Shi, "A cylindrical traveling wave ultrasonic motor using longitudinal and bending composite transducer," *Ferroelectrics*, vol. 409, no. 1, pp. 117–127, 2010.

[20] Y. Liu, L. Wang, Z. Gu, Q. Quan, and J. Deng, "Development of a two-dimensional linear piezoelectric stepping platform using longitudinal-bending hybrid actuators," *IEEE Trans. Ind. Electron.*, vol. 66, no. 4, pp. 3030–3040, Apr. 2019.

[21] J. Deng, Y. Liu, J. Liu, D. Xu, and Y. Wang, "Development of a planar piezoelectric actuator using bending–bending hybrid transducers," *IEEE Trans. Ind. Electron.*, vol. 66, no. 8, pp. 6141–6149, Aug. 2019, doi: 10.1109/tie.2018.2873123.

[22] J. Liu, Y. Liu, L. Zhao, D. Xu, W. Chen, and J. Deng, "Design and experiments of a single-foot linear piezoelectric actuator operated in a stepping mode," *IEEE Trans. Ind. Electron.*, vol. 65, no. 10, pp. 8063–8071, Oct. 2018.

[23] D. Xu, Y. Liu, S. Shi, J. Liu, W. Chen, and L. Wang, "Development of a nonresonant piezoelectric motor with nanometer resolution driving ability," *IEEE/ASME Trans. Mechatronics*, vol. 23, no. 1, pp. 444–451, Feb. 2018.

[24] Q. Pan, Y.-B. Liu, Y.-H. Liu, L.-J. Gong, L.-G. He, and Zhi-H. Feng, "Design and fabrication of a large displacement piezoelectric actuator," in *Proc. Symp. Piezoelectr., Acoustic Waves, Device Appl. (SPAWDA)*, Oct./Nov. 2015, pp. 261–264.
[25] Q. Pan, J. Hu, E. Miao, S. Chen, S. Shu, and P. Hu, "Novel piezoelectric rotary motor driven by a single-phase sine wave with an asymmetric stator," *Rev. Sci. Instrum.*, vol. 90, no. 8, 2019, Art. no. 089902.
[26] Y. Liu, W. Chen, J. Liu, and S. Shi, "A cylindrical traveling wave ultrasonic motor using longitudinal and bending composite transducer," *Sens. Actuators A, Phys.*, vol. 161, nos. 1–2, pp. 158–163, Jun. 2010.
[27] Y. Liu, W. Chen, P. Feng, and J. Liu, "Miniaturization of a U-shape linear piezoelectric motor with double feet," *Sens. Actuators A, Phys.*, vol. 214, pp. 95–100, Aug. 2014.
[28] J. Li, X. Zhou, H. Zhao, M. Shao, Z. Fan, and H. Liu, "Design and experimental tests of a dual-servo piezoelectric nanopositioning stage for rotary motion," *Rev. Sci. Instrum.*, vol. 86, no. 4, Apr. 2015, Art. no. 045002.
[29] Y. Liu, W. Chen, D. Shi, X. Tian, S. Shi, and D. Xu, "Development of a four-feet driving type linear piezoelectric actuator using bolt-clamped transducers," *IEEE Access*, vol. 5, pp. 27162–27171, 2017.
[30] Y. Liu, J. Deng, and Q. Su, "Review on Multi-Degree-of-Freedom piezoelectric motion stage," *IEEE Access*, vol. 6, pp. 59986–60004, 2018.

YONG ZHANG was born in 1965. He is currently an Associate Professor with the School of Instrument Science and Opto-Electronics Engineering, Hefei University of Technology, China. His main research interests include modern precision system testing technology, piezoelectric transducers, motors, and piezoelectric pumps.

TAO XU was born in 1999. He is currently pursuing the B.E. degree with the Hefei University of Technology, China. He is focusing on the piezoelectric materials for novel actuators and sensors, particularly piezoelectric motors.

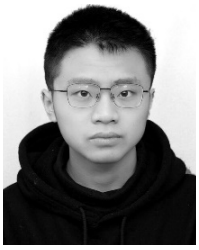

JINSHENG HU was born in 1998. He is currently pursuing the B.E. degree with the Hefei University of Technology, China. He is focusing on the piezoelectric materials for novel actuators and sensors, particularly piezoelectric motors.

ZHEN HUANG was born in 1999. He is currently pursuing the B.E. degree with the Hefei University of Technology, China. He is focusing on the piezoelectric materials for novel actuators and sensors, particularly piezoelectric motors.

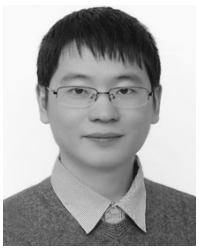

QIAOSHENG PAN was born in 1990. He received the Ph.D. degree from the Department of Precision Machinery and Precision Instrumentation, University of Science and Technology of China (USTC), China, in 2016. He is currently an Assistant Professor with the School of Instrument Science and Opto-Electronics Engineering, Hefei University of Technology, China. His research interests include piezoelectric transducers, piezoelectric motors, and piezoelectric pumps.